

Numerical Diagonalization Study of the Phase Boundaries of the $S = 2$ Heisenberg Antiferromagnet on the Orthogonal Dimer Lattice

Hiroki Nakano¹, Tôru Sakai^{1,2}, and Yuko Hosokoshi³

¹ Graduate School of Science, University of Hyogo, Kamigori, Hyogo 678-1297, Japan

² National Institutes for Quantum and Radiological Science and Technology, SPring-8 Sayo, Hyogo 679-5148, Japan

³ Department of Physics, Osaka Metropolitan University, Osaka 558-8585, Japan

The $S = 2$ Heisenberg antiferromagnet on the orthogonal dimer lattice is studied. The edges of the exact dimer and Néel-ordered phases in the ground state of the system are examined by the numerical diagonalization method. Our present results are discussed by combining them with previously obtained estimates for smaller- S cases. We find that an intermediate region between the exact dimer and Néel-ordered phases gradually widens as spin S is increased up to $S = 2$.

The Heisenberg antiferromagnet on the orthogonal dimer lattice has garnered significant attention as a frustrated magnets, similar to the kagome and triangular lattice antiferromagnets. This orthogonal dimer system is referred to as the Shastry–Sutherland model.¹⁾ The frustration often gives rise to various phase transitions and exotic quantum states. However, notably, the number of quantum states that can be obtained in a mathematically rigorous form is limited. In this situation, the Shastry–Sutherland model serves as a valuable example, wherein the exact dimer ground state is realized when the orthogonal dimer interactions are sufficiently strong. Conversely, the model is in the Néel-ordered phase when the interactions that form the square lattice are adequately strong. The majority of subsequent studies has concentrated on the case of $S = 1/2$. The discovery of $\text{SrCu}_2(\text{BO}_3)_2$ as a good candidate material in Ref. 2 has notably increased the importance of the $S = 1/2$ model. Extensive and intensive studies have been conducted on this system from theoretical and experimental perspectives.^{3–12)} These studies have led to a widespread consensus that $\text{SrCu}_2(\text{BO}_3)_2$ is in the dimer phase of the Shastry–Sutherland model.

However, research on cases in which spin S is greater than $1/2$ is scarce. Shastry and Sutherland¹⁾ demonstrated that the direct product of the two spin states that form a singlet dimer is a rigorous eigenstate of the system, not only in the $S = 1/2$ case but also in larger- S cases. When the dimer interaction J_1 is sufficiently strong, this exact dimer eigenstate is the ground state of the system with the system size N having the energy

$$E_{\text{ED}} = -\frac{1}{2}N J_1 S(S+1). \quad (1)$$

In the case of strong interactions forming the square lattice J_2 , the Néel-ordered phase emerges irrespective of S . According to Kanter,¹³⁾ a rigorous region of the ratio of the interactions as a necessary condition as follows:

$$\frac{J_2}{J_1/2} \leq \frac{1}{S+1}, \quad (2)$$

for $S \geq 1$ and

$$\frac{J_2}{J_1/2} \leq 1, \quad (3)$$

for $S = 1/2$ when the exact singlet dimer state is the ground state. However, this study has been followed by only a lim-

ited number of numerical investigations.^{14,15)} Reference 14 focused on the $S = 1$ case and studied the anisotropy effect in the system; only a single-sized sample including 16 spins was treated in this study. In Ref. 15, for the cases of $S = 1$ and $3/2$, the edges of the exact dimer and Néel-ordered phases for the isotropic case were determined based on calculations for 16- and 20-site clusters.

Returning to the $S = 1/2$ case, it was pointed out that as the J_2 interaction is increased beyond the edge of the exact dimer phase, a plaquette singlet state appears before the Néel-ordered phase occurs.⁶⁾ Theoretical attempts to reliably estimate phase boundaries and deepen our understanding of the system have been undertaken. A few years ago, Ref. 16 showed that the internal structure of the plaquette singlet phase is complex and not uniform. Subsequently, a series of theoretical studies concerning the $S = 1/2$ case were conducted.^{17–22)} High-pressure experiments successfully changed the ratio J_2/J_1 and reached the boundary of the dimer phase.^{23–25)}

Under the context, the aim of the present letter is to clarify the edges of the exact dimer and Néel-ordered phases in the $S = 2$ case of the Shastry–Sutherland model using a computational and unbiased approach. We thereby deepen our understanding of the systematic behavior of the target system from the exact dimer phase to the Néel-ordered phase. This is the purpose of the present study.

The Hamiltonian studied here is given by

$$\mathcal{H} = \sum_{\langle i,j \rangle: \text{orthogonal dimer}} J_1 \mathbf{S}_i \cdot \mathbf{S}_j + \sum_{\langle i,j \rangle: \text{square lattice}} J_2 \mathbf{S}_i \cdot \mathbf{S}_j. \quad (4)$$

Here, \mathbf{S}_i denotes the $S = 2$ spin operator at site i . In this study, we consider the case of an isotropic interaction in the spin space. Site i is assumed to represent a vertex of the square lattice. The number of spin sites is represented by N . The first term of Eq. (4) expresses the orthogonal dimer interactions illustrated by thick solid bonds in Fig. 1. The second term of Eq. (4) expresses the interactions forming the square lattice illustrated by thin solid bonds in Fig. 1. This study considers that the two interactions between the two spins are antiferromagnetic, namely, $J_1 > 0$ and $J_2 > 0$. Energies are measured in units of J_1 . Hereafter, we set $J_1 = 1$. We use r to represent the ratio J_2/J_1 . When $r = 0$, the system is an assembly of isolated dimerized spin models. However, in the limit $r \rightarrow \infty$, the

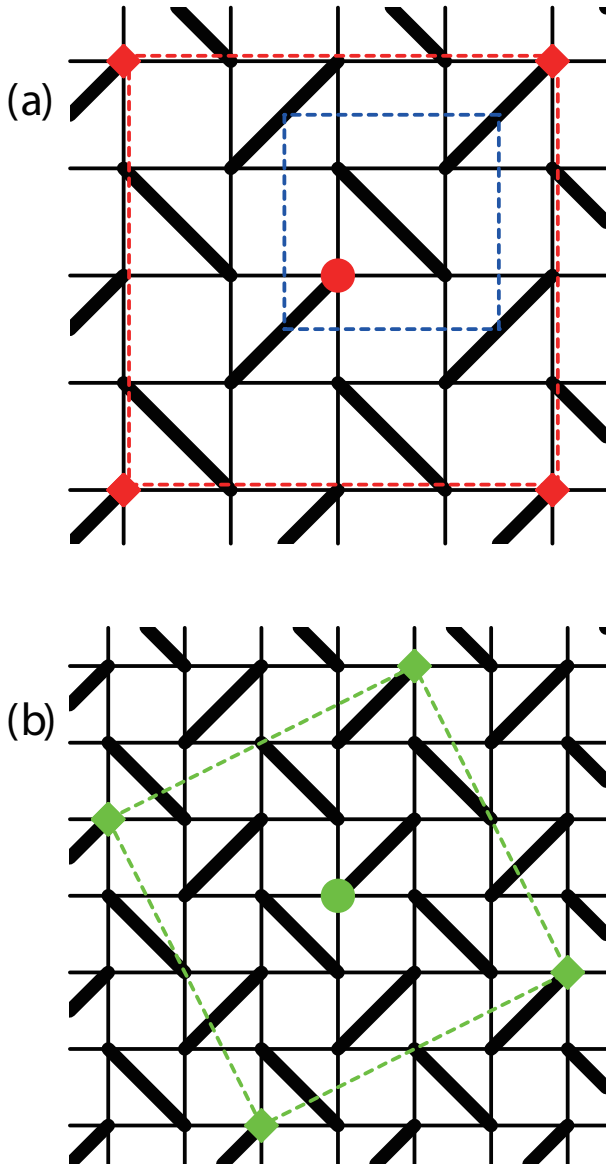


Fig. 1. (Color) Lattice structure of the orthogonal dimer system and finite-sized clusters under the periodic boundary condition. Thick solid lines show the bonds of the orthogonal dimer interaction (J_1). Thin solid lines represent the interaction forming the square lattice (J_2). The case of $N = 16$ is shown by the red broken square in Panel (a) and the unit cell ($N = 4$) is represented by the blue broken square. Note that the red broken square is displayed with a slight translational shift to avoid situations in which overlapping lines make visibility difficult. In Panel (b), the case of $N = 20$ is shown using the green broken lines. The present study investigates the case when $S = 2$ spins are located at each vertex of the square lattice, whereas in Ref. 15, $S = 1$ or $S = 3/2$ spins are located at each vertex. The filled circle in each panel illustrates the center site of the square; filled diamonds illustrate the corners of the square. The pair of the circle and the diamond sites is the longest-distant one in each cluster under the periodic boundary condition.

system is reduced to the $S = 2$ Heisenberg antiferromagnet on the ordinary square lattice. This study examines the ratios of the edges of the exact dimer and Néel-ordered phases denoted by r_{c1} and r_{c2} , respectively.

We examine finite-sized clusters under the periodic boundary condition. This study treats the $N = 16$ and 20 finite-sized clusters illustrated in Fig. 1. Note that $N/4$ is an integer because the number of spins in a unit cell of the present sys-

tem, which is illustrated in Fig. 1(a), is four. Note that these two clusters are regular squares. These regular square clusters help us to capture the essence of the two dimensions of the present system.

We carry out numerical diagonalizations using the Lanczos algorithm to obtain the lowest energy of \mathcal{H} in the subspace belonging to $\sum_j S_j^z = M$. Note that z -axis is taken as the quantized axis of each spin. The prevailing consensus is that numerical diagonalization calculations are unbiased. Consequently, reliable information about the system can be obtained. The energy is represented by $E(N, M)$, where M is an integer between $-NS$ and NS . We mainly focus on the case of $M = 0$ because the ground state energy E_g is given by $E(N, M = 0)$. Some of our Lanczos diagonalizations were carried out using MPI-parallelized code that was originally developed in a study of Haldane gaps.²⁶⁾ The usefulness of our program was confirmed via large-scale parallelized calculations.²⁷⁻²⁹⁾ Note that the dimension of the matrix of the largest-scale calculations in this study is 5,966,636,799,745 in the subspace $M = 0$ for $N = 20$. The calculations have been carried out on Fugaku using 65,105 nodes. To the best of our knowledge, Ref. 27 was the first study in which a numerical diagonalization for an $S = 2$ Heisenberg antiferromagnet of $N = 20$ size was carried out to investigate the Haldane gap issue for a one-dimensional system. However, the computational cost of the $S = 2$ system with $N = 20$ still remains substantial even when using Fugaku. Our program was confirmed to succeed in treating systems with even larger matrix dimensions (12,663,809,507,129 in Ref. 28, 18,252,025,766,941 in Ref. 29, and 32,247,603,683,100 in Ref. 21) using Fugaku. Because the dimension for the $S = 2$ case of $N = 24$, which is the next larger target of the present study, is more than 10^{15} , its numerical diagonalization calculations are difficult in the present computational environment.

First, we observe an r -dependence of E_g near the edge of the exact dimer phase in the results depicted in Fig. 2. Panels (a) and (b) correspond to the $N = 16$ and 20 cases, respectively. In each panel, one can observe that our calculations successfully capture the energy level ($E_g/J_1 = -3N$) of the exact dimer state in the region of small r . In the region where r becomes larger than a specific value, E_g becomes lower than the exact dimer state. In each panel, we draw a fitting line determined from two data points which are close to the energy level of the exact dimer state. Note that other large- r data points that are not used for the fitting fall on the fitting line. Our calculations strongly suggest that a spin state that is different from the exact dimer state exists in the range of large r in Fig. 2. The intersection of the horizontal solid line and the broken fitting line provides information about the edge of the exact dimer phase. Our results for the intersection are

$$r = 0.2731, \quad (5)$$

for $N = 16$ and

$$r = 0.2807, \quad (6)$$

for $N = 20$. The difference between the two results (5) and (6) is small. These results suggest that the edge of the exact dimer phase is

$$r_{c1} = 0.28(1). \quad (7)$$

Subsequent analyses will compare this result (7) with previ-

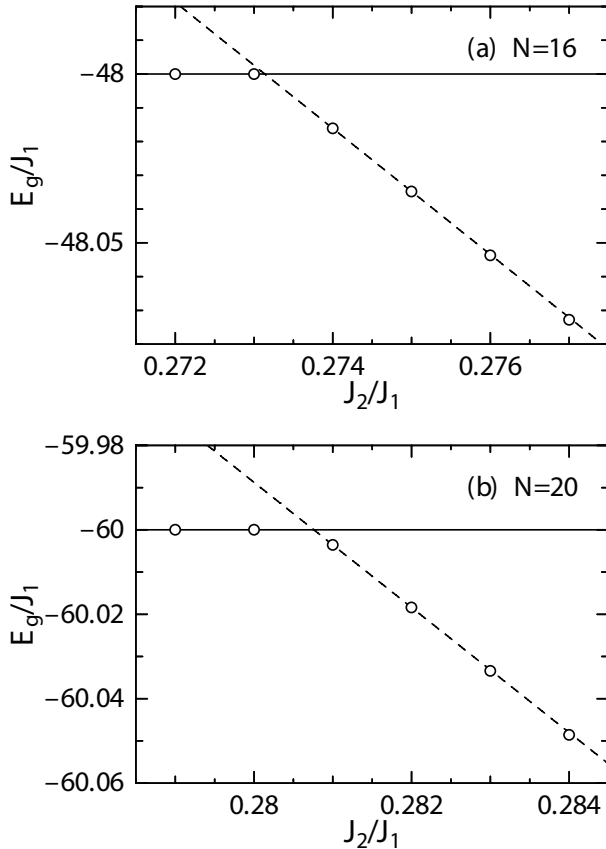


Fig. 2. Ground state energy of the $S = 2$ orthogonal dimer lattice anti-ferromagnet near the edge of the exact dimer phase. Circles represent our numerical diagonalization results for $N = 16$ and 20 in panels (a) and (b), respectively. The horizontal solid line shows the energy of the exact dimer state. The broken line in each panel is obtained by fitting based on the two points that are close to the energy level of the exact dimer state.

ously reported results for smaller- S .

Next, we examine the edge of the Néel-ordered phase by observing the spin correlation functions in the ground state. We focus on $\langle S_i^z S_j^z \rangle$ for a pair of i and j of the longest distance in the finite-sized clusters. This quantity helps us to know whether the system exhibits the Néel order. The longest distance is then determined as the distance from the center of the regular square to each corner of the regular square, as illustrated in Fig. 1. Analysis of the correlation function for the longest-distance pair was also carried out in a study based on Monte Carlo simulations.³⁰⁾ The present results are depicted in Fig. 3 together with the results of $S = 3/2$ in Ref. 15 for comparison. The results for $N = 16$ over the entire range are presented. Above $r \sim 0.68$, $\langle S_i^z S_j^z \rangle$ takes values that are significantly larger than unity. When r is decreased from $r \sim 0.68$ to $r \sim 0.67$, $\langle S_i^z S_j^z \rangle$ rapidly but continuously decreases. It also shows discontinuous behavior at the ratio expressed in Eq. (5). However, for $N = 20$, we concentrate on carrying out our large-scale calculations only for the cases for $r = 0.65, 0.67$, and 0.68 because the corresponding computational jobs consume many node-hour products as computational resources. One finds that $\langle S_i^z S_j^z \rangle$ of $N = 20$ for $r = 0.67$ and 0.68 take values that agree with $\langle S_i^z S_j^z \rangle$ for $N = 16$ above $r \sim 0.68$. On the other hand, $\langle S_i^z S_j^z \rangle$ for $N = 20$ for $r = 0.65$ takes a negative value; its absolute value is approximately 50% of the absolute value of $\langle S_i^z S_j^z \rangle$ of $N = 16$. This behavior is shared with

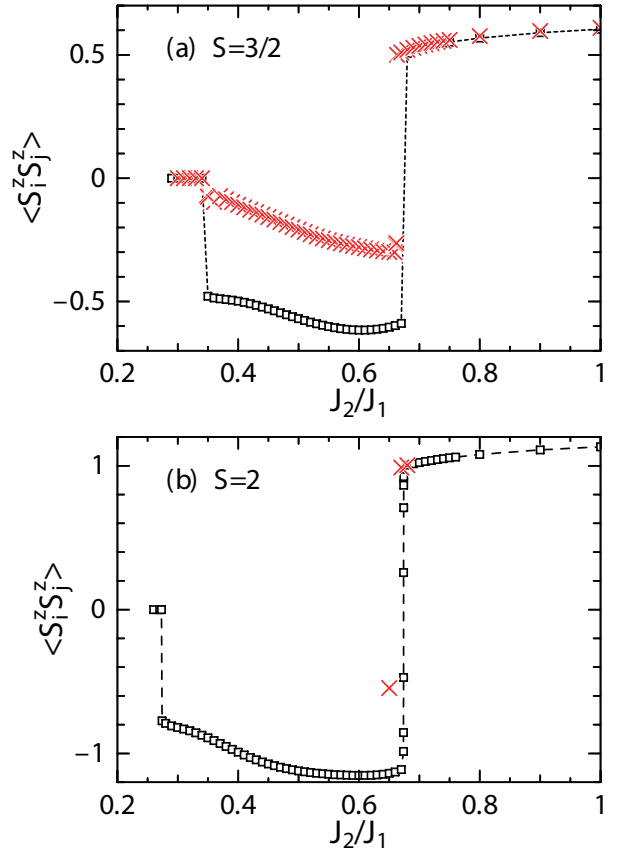


Fig. 3. (Color) Correlation function $\langle S_i^z S_j^z \rangle$ for the pair of i and j with the longest distance in each finite-sized cluster. Squares and crosses denote the results for $N = 16$ and 20, respectively. Panels (a) and (b) show the results for $S = 3/2$ and 2, respectively. Panel (a) is reproduced from Ref. 15 so that readers can easily identify the similarities and differences between the $S = 3/2$ and $S = 2$ cases.

the case of $S = 3/2$ shown in Fig. 3(a). Therefore, our calculations strongly suggest that the edge of the Néel-ordered phase is located at

$$r_{c2} = 0.66(2). \quad (8)$$

The result will next be compared with previously reported results for smaller- S .

Now, let us combine the present results for $S = 2$ and the results for smaller- S cases reported previously to capture the systematic behaviors of r_{c1} and r_{c2} as functions of $1/S$. The results are depicted in Fig. 4, where the data for $S = 1$ and $3/2$ are taken from Ref. 15, the data of r_{c1} for $S = 1/2$ from Ref. 21, and the data of r_{c2} for $S = 1/2$ from Ref. 16. One can observe that r_{c1} gradually decreases as S is increased and that r_{c1} seems to vanish within the limit of $S \rightarrow \infty$. Our present result for the region of the exact dimer ground state is significantly wider than the region expressed using Inequality (2). On the other hand, the decrease for r_{c2} with increasing S seems monotonic and extremely small. Even in the limit of $S \rightarrow \infty$, r_{c2} appears to remain nonzero. The boundaries of the exact dimer and Néel-ordered phases were examined in Ref. 8, where the author treated a generalized Hamiltonian to $\text{Sp}(2n)$ symmetry and argued for properties under the large- n limit. Reference 8 reported that the boundary of the (π, π) long-range order phase is almost fixed at $J_2/J_1 = 1$. This fixed boundary is similar to our results showing that a small

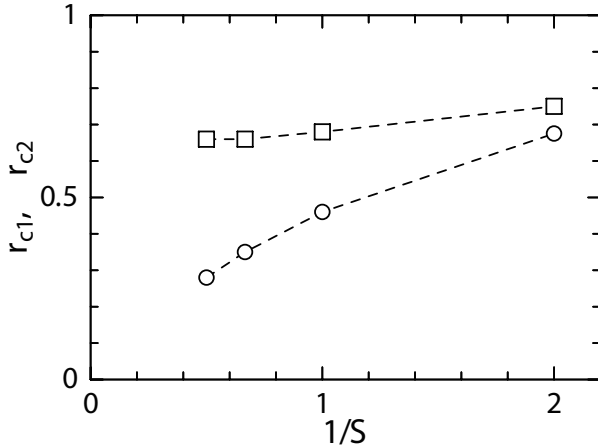


Fig. 4. S -dependence of r_{c1} and r_{c2} . Circles and squares denote the results for r_{c1} and r_{c2} , respectively, where r_{c1} and r_{c2} are the edges of the exact dimer and Néel-ordered phases.

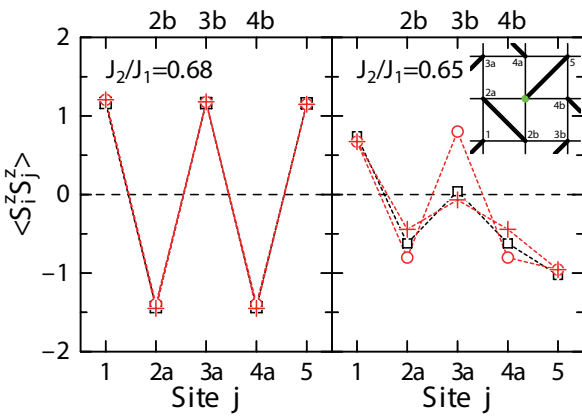


Fig. 5. (Color) Correlation function $\langle S_i^z S_j^z \rangle$ for the pair of an arbitrary site i and j that is within short-range distance. The inset shows the numbering of site j around site i illustrated by a filled green circle. The results for $N = 16$ are plotted as black open squares and those for $N = 20$ are plotted as red open circles and pluses, for $j = 2a, 3a, 4a$ and $j = 2b, 3b, 4b$, respectively.

decrease in r_{c2} occurs with increasing S . However, our present result for Néel-ordered phase is considerably wider than that in Ref. 8. In addition, our present result for the region of the exact dimer ground state is also wider than that of the dimer short-range order phase in Ref. 8. Therefore, the present results for the intermediate region between the exact dimer and Néel-ordered phases is narrower than that of the (π, q) long-range order phase between the (π, π) long-range order and the dimer short-range order phases in Ref. 8. Our narrower intermediate region based on an unbiased Lanczos-diagonalization study of the SU(2) Hamiltonian suggests that the ground state energy of the spin- S Heisenberg antiferromagnet on the orthogonal dimer lattice in the intermediate region is not as low as the corresponding energy of the generalized Hamiltonian in the large- n limit.

Finally, to capture the properties of the spin state of the system in the intermediate region, let us observe $\langle S_i^z S_j^z \rangle$ for the pair of i and j that are close to each other. The results are depicted in Fig. 5. Note that the numerical results for the finite-sized cluster with $N = 20$ show difference between $j = 1 \rightarrow$

$2a \rightarrow 3a \rightarrow 4a \rightarrow 5$ and $j = 1 \rightarrow 2b \rightarrow 3b \rightarrow 4b \rightarrow 5$ because of the tilt of the square of $N = 20$ although no difference occurs in the $N = 16$ case without tilting. For $J_2/J_1 = 0.68$, one can clearly observe a staggered behavior in our numerical data, namely, $\langle S_i^z S_j^z \rangle$ are negative for $j = 2a, 2b, 4a$, and $4b$, whereas $\langle S_i^z S_j^z \rangle$ are all positive for $j = 1, 3a, 3b$, and 5 . The staggered orientations of spins are related to the result of $\langle S_i^z S_j^z \rangle$ for the longest-distant pair for $J_2/J_1 = 0.68$ as shown in Fig. 3(b). By contrast, all the results of $|\langle S_i^z S_j^z \rangle|$ for $J_2/J_1 = 0.65$ become smaller than those for $J_2/J_1 = 0.68$. For $J_2/J_1 = 0.65$, the results for $\langle S_i^z S_j^z \rangle$ for $j = 2a, 2b, 4a$, and $4b$ as a nearest-neighbor pair in the square lattice show negative values. For $j = 5$, $\langle S_i^z S_j^z \rangle$ becomes negative, which suggests that the J_2 interactions disturb the staggered orientation of spins. Between $j = 3a$ and $3b$, a significant difference emerges for $N = 20$. For $j = 1$, the positive values of $\langle S_i^z S_j^z \rangle$ are maintained from $J_2/J_1 = 0.68$ to $J_2/J_1 = 0.65$. Consequently, the staggered nature survives for $J_2/J_1 = 0.65$ only within the range up to the nearest-neighbor pair. Our investigation does not thoroughly clarify properties of the ground state in the intermediate region. Characteristics of the system in the intermediate region should be examined carefully in future.

In summary, we have studied the $S = 2$ Heisenberg antiferromagnet on the orthogonal dimer lattice. The edges of the exact dimer phase r_{c1} and Néel-ordered phase r_{c2} have been obtained by applying the Lanczos diagonalization method to finite-sized clusters with system sizes $N = 16$ and 20 . Our results for r_{c1} and r_{c2} suggest that an intermediate region appears between the two phases, which is wider than those for smaller- S cases. Properties of the system in the intermediate region will be further investigated in future studies. Such studies will greatly advance our fundamental understanding of frustrated magnetism.

Acknowledgment

We wish to thank Professor N. Todoroki for fruitful discussions. This research was partly supported by KAKENHI (Grants Nos. 20K03866, 23K11125, 23K25824, and 25K07229). In this research, we used the computational resources of the supercomputer Fugaku provided by RIKEN through the HPCI System Research projects (Project IDs: hp220043, hp230114, hp230532, hp230537, and hp250164). Some of the computations were performed using the facilities of the Institute for Solid State Physics, The University of Tokyo and Supercomputing Division, Information Technology Center, The University of Tokyo. This research partly used computational resources of Pegasus provided by Multidisciplinary Cooperative Research Program in Center for Computational Sciences, University of Tsukuba.

- 1) B. S. Shastry and B. Sutherland, *Physica B & C* **108B**, 1069 (1981).
- 2) H. Kageyama, K. Yoshimura, R. Stern, N.V. Marshnikov, K. Onizuka, M. Kato, K. Kosuge, C. P. Slichter, T. Goto, and Y. Ueda, *Phys. Rev. Lett.* **82**, 3168 (1999).
- 3) M. Albrecht and F. Mila, *Europhys. Lett.* **34**, 145 (1996).
- 4) S. Miyahara and K. Ueda, *Phys. Rev. Lett.* **82**, 3701 (1999).
- 5) Z. Weihong, C. J. Hamer, and J. Oitmaa, *Phys. Rev. B* **60**, 6608 (1999).
- 6) A. Koga and N. Kawakami, *Phys. Rev. Lett.* **84**, 4461 (2000).
- 7) Y. Fukumoto, *J. Phys. Soc. Jpn.* **69**, 2755 (2000).
- 8) C. H. Chung, J. B. Marston, and S. Sachdev, *Phys. Rev. B* **64**, 134407 (2001).

9) A. Läuchli, S. Wessel, and M. Sigrist, Phys. Rev. B **66**, 014401 (2002).

10) J. Lou, T. Suzuki, K. Harada, and N. Kawashima, arXiv:1212.1999.

11) P. Corboz and F. Mila, Phys. Rev. B **87**, 115144 (2013).

12) Z. Wang and C. D. Batista, Phys. Rev. Lett. **120**, 247201 (2018).

13) I. Kanter, Phys. Rev. B **39**, 7270 (1989).

14) A. Koga, N. Kawakami, and M. Sigrist, J. Phys. Soc. Jpn. **72**, 938 (2003).

15) H. Nakano and T. Sakai, J. Phys.: Condens. Matter **36**, 455805 (2024).

16) H. Nakano and T. Sakai, J. Phys. Soc. Jpn. **87**, 123702 (2018).

17) J. Y. Lee, Y.-Z. You, S. Sachdev, and A. Vishwanath, Phys. Rev. X **9**, 041037 (2019).

18) T. Shimokawa, Phys. Rev. B **103**, 134419 (2021).

19) J. Yang, A. W. Sandvik, and L. Wang, Phys. Rev. B **105**, L060409 (2022).

20) T. Sakai, R. Furuchi, and H. Nakano, JPS Conf. Proc. **38**, 011155 (2023).

21) H. Nakano and T. Sakai, JPS Conf. Proc. **38**, 011166 (2023).

22) K. Liu and F. Wang, Phys. Rev. B **109**, 134409 (2024).

23) H. Ohta, T. Sakurai, R. Matsui, K. Kawasaki, Y. Hirao, S. Okubo, K. Matsubayashi, Y. Uwatoko, K. Kudo, and Y. Koike, J. Phys. Chem. B **119**, 13755 (2015).

24) M. E. Zayed, Ch. Rüegg, J. Larrea J., A. M. Läuchli, C. Panagopoulos, S. S. Saxena, M. Ellerby, D. F. McMorrow, Th. Strässle, S. Klotz, G. Hamel, R. A. Sadykov, V. Pomjakushin, M. Boehm, M. Jiménez-Ruiz, A. Schneidewind, E. Pomjakushina, M. Stingaciu, K. Conder, and H. M. Rønnow, Nature Physics, **13**, 962 (2017).

25) T. Sakurai, Y. Hirao, K. Hijii, S. Okubo, H. Ohta, Y. Uwatoko, K. Kudo, and Y. Koike, J. Phys. Soc. Jpn. **87**, 033701 (2018).

26) H. Nakano, and A. Terai, J. Phys. Soc. Jpn. **78**, 014003 (2009).

27) H. Nakano, and T. Sakai, J. Phys. Soc. Jpn. **87**, 105002 (2018).

28) H. Nakano, N. Todoroki and T. Sakai, J. Phys. Soc. Jpn. **88**, 114702 (2019).

29) H. Nakano, H. Tadano, N. Todoroki, and T. Sakai, J. Phys. Soc. Jpn. **91**, 074701 (2022).

30) A. W. Sandvik and H. G. Evertz, Phys. Rev. B **82**, 024407 (2010).